

Rates of neutrino conversion and decay in hot and dense QED plasma

Asida N.*

Hukuyama City Junior College for Women, Hiroshima-ken Hukuyama-si

Kita-Honzyoo 720-0074, JAPAN

A. Niégawa[†] and H. Ozaki[‡]

Department of Physics, Osaka City University, Sumiyoshi-ku, Osaka 558-8585, JAPAN

M. Kubota

Hitachi Software Engineering Co., Ltd., Naka-ku, Yokohama 231-0015, JAPAN

Abstract

Using a real-time formalism of equilibrium and nonequilibrium quantum-field theory, we derive the reaction-rate formula for neutrino-conversion ($\nu \rightarrow \nu'$) process and $\nu\bar{\nu}'$ annihilation process, which take place in a hot and dense QED plasma with background (anti)neutrinos out of equilibrium. Also derived is the formula for the inverse processes to the above ones. Using the hard-thermal-loop resummation scheme, we include the contribution from the coherent processes. The decay/production of a neutrino causes an evolution of its spatial distribution. A scheme for dealing with this evolution is presented. For the case of isotropic

*Electronic address: asida@yukawa.kyoto-u.ac.jp

†Electronic address: niegawa@sci.osaka-cu.ac.jp

‡Electronic address: hozaki@sci.osaka-cu.ac.jp

neutrino distribution, numerical computation is carried out for the parameter region of type-II super-nova explosion. Differential reaction rate exhibits characteristic peak structure, which comes from the coherent processes. The contribution from the above processes to the decay or damping rate of a parent neutrino ν is also studied.

11.10.Wx, 13.10.+q, 13.15.+g, 13.35.Hb

I. INTRODUCTION

For the past two decades, properties of neutrinos in background media have attracted much interest (see, e.g., [1]). Interactions of neutrinos with a thermal background cause a change in the properties of neutrinos. The dispersion relation is the quantity that describes this change. Nötzold and Raffelt [2] were the first who comprehensively analyzed the dispersion relation of a neutrino in a thermal background, where, among others, the damping rate of an electron neutrino is computed, the rate which is related to the mean-free path and to the refractive index. Computation is performed by neglecting Pauli blocking effects and using the bare dispersion relation for participating electrons. Radiative decay of a massive neutrino has been analyzed in [3].

It is by now well known [4,5] that, in hot and/or dense QED, the thermal propagators of a soft photon[§] and a soft electron (positron) are drastically changed from those of respective bare counterparts. The salient feature is the appearance of the imaginary part in space-like-momentum region, which comes from Landau damping mechanism. The dispersion relations for soft photon and electron are also largely changed. An effective or improved

[§]A soft particle is the particle that carries soft momentum Q^μ ($|Q^\mu| = O(e\sqrt{T^2 + \mu^2})$). Here $-e$ is the electron charge and T (μ) denotes the temperature (chemical potential).

perturbation theory, called hard-thermal-loop (HTL) resummation scheme [4,5], in which the above-mentioned effects are taken into account, is established just after the work [2].

Recently, in relation to the possible neutrino oscillation, neutrino–conversion processes have attracted much interest. For instance, in [6], the rate of neutrino conversion $\nu_L \rightarrow \nu_R$ in a hot and dense QED (or electron–positron–photon) plasma is computed using the above-mentioned effective perturbation theory. The responsible interaction is the magnetic dipole neutrino-photon interaction. ν_L is assumed to be thermally distributed in the QED plasma.

In this paper, we deal with a neutrino-conversion ($\nu \rightarrow \nu'$) process and a $\nu\bar{\nu}'$ annihilation process, which take place in a hot and dense QED plasma. We also deal with inverse processes to them. The background (anti)neutrinos are out of equilibrium. In Sec. II, we derive the reaction-rate formula for these processes, on the basis of the nonequilibrium quantum-field theory (outlined in Appendix A) supplemented with the effective perturbation theory of hot and dense QED. Also presented is a procedure of determining spacetime evolution of (anti)neutrino distribution function. In Sec. III, for the purpose of illustration, numerical computation is carried out for the differential reaction rate for the case of isotropic neutrino distribution. We are interested in the temperature and baryon-number density regions of type-II supernova explosion (cf. [4,7]); $m_e \ll T$, $\mu \ll m_{ion}$. As in [3,6], we neglect the effect of the ions. The contribution from the coherent processes exhibits a characteristic peak structure in energy distribution of a “decay neutrino” — ν' for the neutrino-conversion process and $\bar{\nu}'$ for the $\nu\bar{\nu}'$ annihilation process. We then study the contribution to the damping rate of ν . Numerical computation is carried out for the case where no neutrino exists in background. Section IV is devoted to discussions. In Appendix A, we present a formalism for dealing with neutrinos in out of equilibrium system, which is used in the main text. In Appendix B, we give the form for the self-energy-part-resummed photon propagator. Finally, in Appendix C, we compute the necessary quantities for the present study.

II. REACTION-RATE FORMULA AND DAMPING RATE OF A NEUTRINO

A. Neutrino-conversion process

We deal with the system that consists of a hot and dense QED plasma and neutrinos. We assume that the QED plasma is in thermal and chemical equilibrium, while the background neutrinos are not. Then, the whole system is out of equilibrium. A neutrino-conversion process of our concern is

$$\nu(K) + \text{QED plasma} \rightarrow \nu'(K') + \text{anything}. \quad (1)$$

We assume that ν is massive, left-handed neutrino (with mass m), ν' is massless and left-handed. The four-momenta K and K' are $K = (E, \mathbf{k})$ with $E = \sqrt{k^2 + m^2}$ and $K' = (k', \mathbf{k}')$, respectively. The QED plasma is assumed to be at rest. The total reaction rate for the process (1) contributes to the damping or “decay” rate Γ_d of a parent neutrino ν . Γ_d also receives a contribution from the relative process to (1),

$$\nu(K) + \bar{\nu}'(-K') + \text{QED plasma} \rightarrow \text{anything}, \quad (2)$$

where $\bar{\nu}'$ is an antiparticle of ν' and $-K' = (k', -\mathbf{k}')$.

The region for various parameters of our interest is

$$T, \mu, E, k', m_e \ll M_W \quad \text{and} \quad m < 2m_e. \quad (3)$$

Here M_W (m_e) is the mass of W boson (electron). We expect that, in the region (3), the result is insensitive to m ($< m_e$). As a matter of fact, we have confirmed that, at least in the range $0 \leq m \leq 100 \text{ eV}/c^2$ [8], no visible change is detected in the results to be given in Sec. III. Thus, we set $m = 0$ throughout in the sequel, so that $K = (k, \mathbf{k})$. In the region (3), we may use the effective Lagrangian, which, after Fierz transformation, reads

$$\mathcal{L}_{\text{eff}} = -2\sqrt{2}G [(\underline{\bar{\nu}}' \gamma^\mu L \underline{\nu}) (\underline{\bar{e}} \gamma_\mu L \underline{e}) + \text{h.c.}].$$

Here $L \equiv (1 - \gamma_5)/2$, G is Fermi’s constant, and underlined fields stand for the fields *in the “weak-interaction basis”*.

For the QED sector, we employ the real-time formalism of equilibrium QED [4,9] and, for the neutrino sector, we use the nonequilibrium real-time formalism of quantum-field theory [10]. Γ_d is written as [10,11]

$$\Gamma_d = |U_{e\nu}^* U_{e\nu'}|^2 \tilde{\Gamma}_d, \quad (4)$$

$$\tilde{\Gamma}_d = -\frac{i}{2k} \text{Tr} \left[L K \Sigma_{21}^{(\nu)}(X; K) \right], \quad (5)$$

$$= \int_{-\infty}^{+\infty} dq_0 \frac{d\tilde{\Gamma}_d}{dq_0}, \quad (6)$$

where U is the lepton mixing matrix and $\Sigma_{21}^{(\nu)}$ is the (21)-element of the 2×2 matrix self-energy part $\hat{\Sigma}_\nu(X; K)$ of nonequilibrium ν . (Here and in the following, “ $\hat{}$ ” denotes 2×2 matrix in a “type-space” [4,9–11].) X stands for the spacetime coordinates of the center of the region, where the reaction takes place, the definition of which is given shortly. The $O(G^2)$ contribution to $\tilde{\Gamma}_d$, $\tilde{\Gamma}_d^{(1)}$, reads [10,11]

$$\begin{aligned} \tilde{\Gamma}_d^{(1)} = & -\frac{1}{2k} \int \frac{d^4 Q}{(2\pi)^4} \Pi_{21}^{(W)\alpha\beta}(Q) \\ & \times \text{Tr} \left[L K \gamma_\alpha S_{21}^{(\nu')}(X; K - Q) \gamma_\beta L \right], \end{aligned} \quad (7)$$

where $\Pi_{21}^{(W)\alpha\beta}$ is the (21) element of the one-loop matrix function $\hat{\Pi}_W^{\alpha\beta}$ whose (ij) element is

$$\begin{aligned} \Pi_{ij}^{(W)\alpha\beta}(Q) = & 8iG^2(-)^{i+j} \int \frac{d^4 P}{(2\pi)^4} \text{Tr} \left[S_{ji}^{(e)}(P - Q) \right. \\ & \left. \times \gamma^\alpha L S_{ij}^{(e)}(P) \gamma^\beta L \right] \\ & (i, j = 1, 2). \end{aligned} \quad (8)$$

The diagrammatic representation of $\tilde{\Gamma}_d^{(1)}$ is given in Fig. 1. In Eq. (8), no summation is taken over i and j . In Eq. (7), $S_{21}^{(\nu')}(X; P)$ is the (21) element of the matrix propagator $\hat{S}_{\nu'}(X; P)$ of out of equilibrium ν' , which is a Wigner transform of its configuration-space counterpart, $\hat{S}_{\nu'}(x, y)$:

$$\hat{S}_{\nu'}(x, y) = \int \frac{d^4 P}{(2\pi)^4} e^{-iP \cdot (x-y)} \hat{S}_{\nu'}(X; P),$$

where $X \equiv (x+y)/2$. $S_{ij}^{(e)}$ in Eq. (8) is the (ij) element of an equilibrium electron propagator matrix \hat{S}_e .

Neutrino sector

From now on, we restrict our concern to the systems, in which the distributions of (anti)neutrinos are of quasi-uniform near equilibrium or of quasistationary. For such systems, the gradient approximation in the derivative expansion is sensible [10]. A brief derivation of $\hat{S}_{\nu'}(X; P)$ to the gradient approximation is given in Appendix A: $\hat{S}_{\nu'}(X; P) = \hat{S}_{\nu'}^{(0)}(X; P) + \hat{S}_{\nu'}^{(1)}(X; P)$ with $\hat{S}_{\nu'}^{(0)}$ the leading term and $\hat{S}_{\nu'}^{(1)}$ the nonleading or gradient term. $\hat{S}_{\nu'}^{(0)}(X; P)$ reads

$$\begin{aligned} \hat{S}_{\nu'}^{(0)}(X; P) &= L\hat{\mathcal{P}}\hat{S}_{\nu'}^{(0)}(X; P), \\ \hat{S}_{\nu'}^{(0)}(X; P) &= \begin{pmatrix} \Delta_R(P) & 0 \\ \Delta_R(P) - \Delta_A(P) & -\Delta_A(P) \end{pmatrix} \\ &\quad + 2\pi i\epsilon(p_0)f_{\nu'}(X; P)\delta(P^2)\hat{A}_+, \end{aligned} \quad (9)$$

where

$$\Delta_{R(A)}(P) = \frac{1}{P^2 \pm i\epsilon(p_0)0^+}, \quad (10)$$

$$\begin{aligned} f_{\nu'}(X; P) &= \theta(p_0)N_{\nu'}(X; p_0, \mathbf{p}) \\ &\quad + \theta(-p_0)[1 - N_{\bar{\nu}'}(X; |p_0|, -\mathbf{p})], \end{aligned} \quad (11)$$

$$\hat{A}_{\pm} = \begin{pmatrix} 1 & \pm 1 \\ \pm 1 & 1 \end{pmatrix}. \quad (12)$$

Here $N_{\nu'}(X; p_0, \mathbf{p})$ [$N_{\bar{\nu}'}(X; |p_0|, -\mathbf{p})$] is the number-density function of ν' [$\bar{\nu}'$] at the space-time point X with “energy” $|p_0|$ and momentum \mathbf{p} [$-\mathbf{p}$]. The nonleading term $\hat{S}_{\nu'}^{(1)}(X; P)$ is given in Eq. (A2) with ν' for ν . In our formalism outlined in Appendix A, $\hat{S}_{\nu'}^{(1)}$ is $O(G^2)$ smaller than $\hat{S}_{\nu'}^{(0)}$. This is because $\hat{S}_{\nu'}^{(1)}$ includes $\partial_{X_\mu}f_{\nu'}(X; P)$, which, as seen from Eq. (34) (with ν' for ν), is proportional to G^2 since so is $F_{\nu'}$. Then, for $S_{21}^{(\nu')}$ in Eq. (7), we substitute the (21) element of the leading term $\hat{S}_{\nu'}^{(0)}$ (Eq. (9)).

Electron sector

The electron propagator matrix $\hat{S}_e(P)$, whose elements are in Eq. (8), is of the form

$$\hat{S}_e(P) = \not{P} \hat{S}_e(P). \quad (13)$$

Here $\hat{S}_e(P)$ is given by the right-hand side (RHS) of Eq. (9) provided that $f_{\nu'}(X;P)$ is replaced by an equilibrium distribution function

$$\begin{aligned} f_e(p_0) &= \theta(p_0)N_e(p_0) + \theta(-p_0)[1 - N_{e^+}(p_0)], \\ N_e(p_0) &= \frac{1}{e^{(p_0-\mu)/T} + 1}, \\ N_{e^+}(p_0) &= \frac{1}{e^{(|p_0|+\mu)/T} + 1}. \end{aligned} \quad (14)$$

We decompose $\Pi_{ij}^{(W)\alpha\beta}(Q)$, Eq. (8), into transverse (T), longitudinal (L), and vector–axial-vector interference (VA) parts. T - and L - parts are proportional to the thermal self-energy part of a photon in hot and dense QCD. Thus, we may write

$$\begin{aligned} \Pi_{ij}^{(W)\alpha\beta}(Q) &= 4\frac{G^2}{e^2} \left[\mathcal{P}_T^{\alpha\beta}(\hat{\mathbf{q}}) \Pi_{ij}^{(T)}(Q) + \mathcal{P}_L^{\alpha\beta}(Q) \Pi_{ij}^{(L)}(Q) \right. \\ &\quad \left. - i\epsilon^{\alpha\beta\rho 0} Q_\rho \Pi_{ij}^{(VA)}(Q) \right], \\ \Pi_{ij}^{(VA)}(Q) &= 2ie^2 \frac{Q^2}{q^2} \int \frac{d^4P}{(2\pi)^4} (q_0 - 2p_0) \\ &\quad \times \mathcal{S}_{ji}^{(e)}(P - Q) \mathcal{S}_{ij}^{(e)}(P), \end{aligned} \quad (15)$$

where $\epsilon^{\mu\nu\rho\sigma}$ is a fully anti-symmetric pseudo tensor with $\epsilon^{0123} = 1$, $\mathcal{S}_{ij}^{(e)}$ ($i, j = 1, 2$) is the (ij) element of \hat{S}_e in Eq. (13), and $\mathcal{P}_{T(L)}^{\alpha\beta}$ is the standard projection operator onto transverse (longitudinal) mode,

$$\begin{aligned} \mathcal{P}_T^{\alpha\beta}(\hat{\mathbf{q}}) &= - \sum_{i,j=1}^3 g^{\alpha i} g^{\beta j} (\delta^{ij} - \hat{q}^i \hat{q}^j) \quad (\hat{q}^i \equiv q^i/q), \\ \mathcal{P}_L^{\alpha\beta}(Q) &= g^{\alpha\beta} - \frac{Q^\alpha Q^\beta}{Q^2} - \mathcal{P}_T^{\alpha\beta}(\hat{\mathbf{q}}). \end{aligned} \quad (16)$$

$\Pi_{ij}^{(T/L)}(Q)$ in Eq. (15) is the (ij) element of the T/L -component of the thermal self-energy part of a photon.

$\Pi_{21}^{(S)}(Q)$ ($S = T, L, VA$) are related to [4,9] the so-called Feynman self-energy part

$$\begin{aligned} \Pi_F^{(S)}(Q) &\equiv \Pi_{11}^{(S)}(Q) + \theta(q_0)\Pi_{12}^{(S)}(Q) + \theta(-q_0)\Pi_{21}^{(S)}(Q) \\ &\quad (S = T, L, VA), \end{aligned} \quad (17)$$

through

$$i\Pi_{21(12)}^{(S)}(Q) = 2[\theta(\pm q_0) + n_B(|q_0|)] \text{Im}\Pi_F^{(S)}(Q) \quad (S = T, L, VA). \quad (18)$$

Here $n_B(x) = 1/(e^{x/T} - 1)$ and “Im” means to take the imaginary part with Feynman prescription. In Appendix C, $\Pi_F^{(S)}$ ($S = T, L, VA$) is computed within the approximation $m_e = 0$, which is a good approximation for a plasma with high temperature and/or density, $m_e \ll T, \mu$. In Sec. III, we discuss to what extent the approximation $m_e = 0$ is good one. It is worth mentioning that $\Pi_F^{(VA)}(Q)$ vanishes for vanishing chemical potential, $\mu = 0$.

O(G²) decay-rate formula

As seen from Eq. (9), $S_{21}^{(\nu')}$ ($X; K - Q$) in Eq. (7) involves $f_{\nu'}(X; K - Q)$. Let us write

$$f_{\nu'}(X; K - Q) = f_{\nu'}(X; k - q_0, \mathbf{k} - \mathbf{q}_{\parallel}, -\mathbf{q}_{\perp}),$$

$$\mathbf{q}_{\parallel} \equiv \frac{1}{k^2}(\mathbf{q} \cdot \mathbf{k})\mathbf{k}, \quad \mathbf{q}_{\perp} \equiv \mathbf{q} - \mathbf{q}_{\parallel}.$$

Then we define $\bar{f}_{\nu'}$ through

$$\begin{aligned} & \int \frac{d^4Q}{2\pi} f_{\nu'}(X; K - Q) \mathcal{G}(q_0, \mathbf{q}_{\parallel}) \\ &= \int dq_0 dq \frac{d(\mathbf{q} \cdot \mathbf{k})}{qk} q^2 \bar{f}_{\nu'}(X; k - q_0, \mathbf{k} - \mathbf{q}_{\parallel}) \mathcal{G}(q_0, \mathbf{q}_{\parallel}) \end{aligned} \quad (19)$$

with \mathcal{G} any function of q_0 and \mathbf{q}_{\parallel} .

Using the formulae displayed above, we obtain, after straightforward manipulation, for $d\tilde{\Gamma}_d^{(1)}/dq_0$ to $O(G^2)$ (see Eqs. (6) and (7)),

$$\begin{aligned} \frac{d\tilde{\Gamma}_d^{(1)}}{dq_0} &= \frac{G^2}{\pi^2} \frac{1}{e^2} \frac{1}{k^2} [\theta(q_0) + n_B(|q_0|)] \epsilon(k - q_0) \\ &\times \int_{\mathcal{R}} dq q \left[1 - \bar{f}_{\nu'} \left(X; k - q_0, \left(1 - \frac{q_0}{k} + \frac{Q^2}{2k^2} \right) \mathbf{k} \right) \right] G^{(1)}(Q), \end{aligned} \quad (20)$$

where

$$\begin{aligned}
G^{(1)}(Q) &= \text{Im} \left[H_T(Q) \Pi_F^{(T)}(Q) \right. \\
&\quad \left. + H_L(Q) \Pi_F^{(L)}(Q) - H_{VA}(Q) \Pi_F^{(VA)}(Q) \right],
\end{aligned} \tag{21}$$

$$\begin{aligned}
H_T(Q) &= Q^2 - 2k^2 + \frac{2}{q^2} \left(kq_0 - \frac{Q^2}{2} \right)^2, \\
H_L(Q) &= 2k^2 - \frac{2}{q^2} \left(kq_0 - \frac{Q^2}{2} \right)^2, \\
H_{VA}(Q) &= (q_0 - 2k) Q^2.
\end{aligned}$$

The integration region \mathcal{R} in Eq. (20) is defined as (see Fig. 2)

$$\begin{aligned}
\mathcal{R} &= \mathcal{R}_1 \cup \mathcal{R}_2, \\
\mathcal{R}_1 &: |q_0| \leq q \leq 2k - q_0, \\
\mathcal{R}_2 &: |2k - q_0| \leq q \leq q_0.
\end{aligned}$$

In the region \mathcal{R}_1 [\mathcal{R}_2], $k'_0 = k - q_0 \geq 0$ [$k'_0 < 0$], and then \mathcal{R}_1 [\mathcal{R}_2] is the kinematically allowed region of the reaction (1) [(2)]. At first sight, at $q_0 = 0$, Eq. (20) seems to diverge at $q = 0$. Inspection of the formulae in Appendix C tells us, however, that this is not the case.

B. Neutrino-production process

We now turn to the inverse processes to (1) and to (2):

$$\nu'(K') + \text{QED plasma} \rightarrow \nu(K) + \text{anything}, \tag{22}$$

$$\text{QED plasma} \rightarrow \nu(K) + \bar{\nu}'(-K') + \text{anything}, \tag{23}$$

where $K' = (k', \mathbf{k}')$, $K = (k, \mathbf{k})$, and $-K' = (k', -\mathbf{k})$. The process (22) is a production process of ν due to the reaction of ν' with constituents of the QED plasma and the process (23) is a $\nu\bar{\nu}'$ production process. The reaction-rate formula for these processes is written as

$$\Gamma_p = |U_{e\nu}^* U_{e\nu'}|^2 \tilde{\Gamma}_p, \tag{24}$$

$$\tilde{\Gamma}_p = \frac{i}{2k} \text{Tr} \left[L K \Sigma_{12}^{(\nu)}(X; K) \right], \quad (25)$$

$$= \int_{-\infty}^{+\infty} dq_0 \frac{d\tilde{\Gamma}_p}{dq_0}. \quad (26)$$

In a similar manner as above, we obtain for the $O(G^2)$ contribution,

$$\begin{aligned} \frac{d\tilde{\Gamma}_p^{(1)}}{dq_0} &= -\frac{G^2}{\pi^2} \frac{1}{e^2} \frac{1}{k^2} [\theta(-q_0) + n_B(|q_0|)] \epsilon(q_0 - k) \\ &\times \int_{\mathcal{R}} dq q \bar{f}_{\nu'} \left(X; k - q_0, \left(1 - \frac{q_0}{k} + \frac{Q^2}{2k^2} \right) \mathbf{k} \right) G^{(1)}(Q), \end{aligned} \quad (27)$$

where $\bar{f}_{\nu'}$ is as in Eq. (19) and $G^{(1)}(Q)$ is as in Eq. (21). The diagram for $\tilde{\Gamma}_p^{(1)}$ is the same as Fig. 1, provided that the two types of vertices are interchanged, $1 \leftrightarrow 2$.

C. Contributions from a set of coherent processes

According to the HTL-resummation scheme [5,4], the integration region in Eqs. (6), (20), (26), and (27) should be divided into hard- Q region ($|Q^\mu| = O(\sqrt{T^2 + \mu^2})$) and the soft- Q region ($|Q^\mu| = O(e\sqrt{T^2 + \mu^2})$).

Hard- Q region: For $\text{Im}\Pi_F^{(S)}(Q)$ ($S = T, L, VA$), expressions given in Appendix C are used.

Soft- Q region: Observing the formulae in Appendix C, we see that, for $e \ll 1$,

$$\begin{aligned} H_{T/L}(Q) \text{Im}\Pi_F^{(T/L)}(Q) &\simeq H_{T/L}(Q) \text{Im}F_{T/L}(Q) \\ &\gg H_{VA}(Q) \Pi_{21}^{(VA)}(Q), \end{aligned} \quad (28)$$

where $\text{Im}F_{T/L}(Q)$ is as in Eq. (C1) with Eqs. (C14) and (C15) in Appendix C. In the soft- Q region, there is an additional contribution: An inverse HTL-resummed photon propagator (cf. Eq. (B3)) $\left({}^* \Delta_F^{(T/L)}(Q) \right)^{-1} (= Q^2 - \Pi_F^{(T/L)}(Q) \simeq Q^2 - F_{T/L}(Q))$ is of the same order of magnitude as $\Pi_F^{(T/L)}(Q)$ ($\simeq F_{T/L}(Q)$). Thus, the diagram for $\tilde{\Gamma}_d$ as shown in Fig. 3 yields an equally important contribution.

The characteristic scale of the hard region is [5,4] $\sqrt{T^2 + \mu^2}$, and that of the soft region is $e\sqrt{T^2 + \mu^2}$. As a matter of fact, since $e \simeq 0.30$, the hard region and the soft region are not *sharply separated*. Taking this fact into account, we compute the contribution from Fig. 3,

$\Gamma^{(2)}$, without using the HTL-approximation ($e \ll 1$). The contribution is given by Eq. (7) with the replacement [4,9],

$$\begin{aligned} \Pi_{21}^{(W)\alpha\beta}(Q) &\rightarrow -\frac{e^2}{8G^2} \sum_{i,j=1}^2 \Pi_{2i}^{(W)\alpha\mu}(Q) \\ &\quad \times (*\Delta_{ij}(Q))_{\mu\nu} \Pi_{j1}^{(W)\nu\beta}(Q), \end{aligned} \quad (29)$$

where Π 's are as in Eq. (8) and $*\Delta$ is as in Appendix B. Straightforward computation yields

$$\begin{aligned} \frac{d\tilde{\Gamma}_d^{(2)}}{dq_0} &= \frac{G^2}{\pi^2} \frac{1}{e^2} \frac{1}{k^2} [\theta(q_0) + n_B(|q_0|)] \epsilon(k - q_0) \\ &\quad \times \int_{\mathcal{R}} dq q \left[1 - \bar{f}_{\nu'} \left(X; k - q_0, \left(1 - \frac{q_0}{k} + \frac{Q^2}{2k^2} \right) \mathbf{k} \right) \right] G^{(2)}(Q), \end{aligned} \quad (30)$$

where

$$\begin{aligned} G^{(2)}(Q) &= \frac{1}{2} \text{Im} \left[\sum_{P=T,L} H_P(Q) \frac{(\Pi_F^{(P)}(Q))^2}{Q^2 - \Pi_F^{(P)}(Q)} \right. \\ &\quad \left. + H_T(Q) q^2 \frac{(\Pi_F^{(VA)}(Q))^2}{Q^2 - \Pi_F^{(T)}(Q)} - 2H_{VA}(Q) \frac{\Pi_F^{(T)}(Q) \Pi_F^{(VA)}(Q)}{Q^2 - \Pi_F^{(T)}(Q)} \right]. \end{aligned} \quad (31)$$

The replacement (29) and Fig. 3 tell us [11] that Eq. (30) describes the differential rate for a set of processes, in which real and/or virtual photon(s) participate. It is to be noted that the (real) photons in the QED plasma are in thermal equilibrium. Then, the photon(s) does not come out of the plasma, so that, when the decay neutrino goes out from the plasma, it does not accompany photon(s). [In this relation, see [3]].

In a similar manner, we obtain, for the contribution from the processes (22) and (23),

$$\begin{aligned} \frac{d\tilde{\Gamma}_p^{(2)}}{dq_0} &= -\frac{G^2}{\pi^2} \frac{1}{e^2} \frac{1}{k^2} [\theta(-q_0) + n_B(|q_0|)] \epsilon(q_0 - k) \\ &\quad \times \int_{\mathcal{R}} dq q \bar{f}_{\nu'} \left(X; k - q_0, \left(1 - \frac{q_0}{k} + \frac{Q^2}{2k^2} \right) \mathbf{k} \right) G^{(2)}(Q). \end{aligned} \quad (32)$$

The diagram for this is the same as Fig. 3, provided that the type-1 vertex and the type-2 vertex in Fig. 3 are interchanged.

In the next section, we shall use the formulae displayed above for the whole Q^2 -region.

D. Net decay rate

The net decay rate Γ_d^{net} and the net production rate Γ_p^{net} are

$$\begin{aligned}\Gamma_d^{\text{net}}(X; \mathbf{k}) &= N_\nu(X; \mathbf{k})\Gamma_d(X; \mathbf{k}) \\ &\quad - [1 - N_\nu(X; \mathbf{k})]\Gamma_p(X; \mathbf{k}) \\ &= -\Gamma_p^{\text{net}}(X; \mathbf{k}),\end{aligned}\tag{33}$$

where $N_\nu(X; \mathbf{k})$ is an (on mass-shell) distribution function of ν . When ν , ν' , and $\bar{\nu}'$ are in thermal and chemical equilibrium, N_ν , $N_{\nu'}$, and $N_{\bar{\nu}'}$ take similar form to Eq. (14). Using Eq. (18), one can show, in this case, that the detailed balance holds, $\Gamma_d^{\text{net}}(X; \mathbf{k}) \rightarrow \Gamma_d^{\text{net}}(k) = 0$.

E. Procedure of determining (anti)neutrino distribution functions

Here we study the neutrino or weak-interaction sector. As discussed above after Eq. (12), the nonleading piece of $\hat{S}_{\nu'}$, $\hat{S}_{\nu'}^{(1)}$, is $O(G^2)$ smaller than the leading piece $\hat{S}_{\nu'}^{(0)}$ and may be neglected. Higher-order corrections to $\Sigma_{21}^{(\nu)}$, Eq. (5), and to $\Sigma_{12}^{(\nu)}$, Eq. (25), due to weak interaction, are also $O(G^2)$ smaller than the respective leading contributions analyzed above, so that they can be ignored. There is, however, an exception to this argument. Our formalism outlined in Appendix A accompanies, for each neutrino ν , the evolution equation for f_ν , which is included in the neutrino propagator $\hat{S}_\nu(X; P)$:

$$\not{\partial}_X f_\nu(X; P)L = F_\nu(X; P),\tag{34}$$

$$F_\nu(X; P) = i \left[(1 - f_\nu)\Sigma_{12}^{(\nu)} + f_\nu\Sigma_{21}^{(\nu)} \right].\tag{35}$$

Here $\Sigma_{ij}^{(\nu)}$ is the (ij) element of the self-energy-part matrix $\hat{\Sigma}_\nu$ and is of $O(G^2)$. For computing $F_\nu(X; P)$, all the relevant contributions should be included, among which are the contributions analyzed above. (See Appendix A for more details.)

We show in Appendix A that, on the mass-shell $p_0 = \pm p$, Eq. (34) turns out to the Boltzmann equation (A7) and its relatives, Eqs. (A8) and (A9). As a matter of fact, as far

as $O(G^2)$ contributions are concerned, only f_ν on the mass-shell is relevant because of the presence of $\delta(P^2)$ in Eq. (9). Eq. (34) describes the spacetime evolution of $f_\nu(X; P)$ under a given initial data $f_\nu(X_{\text{in}}^0, \mathbf{X}; P)$ at an initial time $X^0 = X_{\text{in}}^0$. Although the RHS of Eq. (34) is of $O(G^2)$, its effect cannot be ignored in general. This is because, in the process of solving Eq. (34) for $f_\nu(X; P)$, integration over *large spacetime scale* is involved, so that the $O(G^2)$ effect is enhanced.

In conclusion, neutrino self-energy part can be ignored everywhere but in F_ν in Eq. (34). In computing the reaction rates, as dealt with here, one should substitute the (anti)neutrino distribution functions, which are determined through Eq. (34) in a self-consistent manner. This applies to every neutrino.

III. NUMERICAL COMPUTATION

In this section we present a result of numerical computation of the “portion” of $d\tilde{\Gamma}_{d(p)}/dq_0$ and $\tilde{\Gamma}_{d(p)}$ that are independent of the ν' distribution function. We are interested in the type-II supernova environment, which is a QED plasma whose core temperature is $T \sim 30 - 60$ MeV and electron chemical potential is $\mu \sim 350$ MeV [4].

A. Differential reaction rates

In general, the number-distribution function of ν' ($\bar{\nu}'$), $N_{\nu'(\bar{\nu}')} (X; k'_0, \mathbf{k}')$ ($K' = K - Q$), is anisotropic, and one should compute Eqs. (20), (27), (30), and (32) substituting $N_{\nu'}$ and $N_{\bar{\nu}'}$, which are to be determined self consistently. In this section, we restrict ourselves to the case of isotropic distribution, $N_{\nu'(\bar{\nu}')} (k'_0, \mathbf{k}') = N_{\nu'(\bar{\nu}')} (k'_0)$. In this case, Eqs. (20), (27), (30), and (32) may be written in the form,

$$\begin{aligned} \frac{d\tilde{\Gamma}_d^{(i)}}{dq_0} &= \frac{G^2}{\pi^2} \frac{1}{e^2} \frac{1}{k^2} [1 - f_{\nu'}(X; k - q_0)] \\ &\quad \times \mathcal{G}^{(i)}(q_0, k, T) \quad (i = 1, 2), \\ \frac{d\tilde{\Gamma}_p^{(i)}}{dq_0} &= \frac{G^2}{\pi^2} \frac{1}{e^2} \frac{e^{-q_0/T}}{k^2} f_{\nu'}(X; k - q_0) \mathcal{G}^{(i)}(q_0, k, T) \end{aligned}$$

$$(i = 1, 2).$$

Here

$$\begin{aligned} \mathcal{G}^{(i)}(q_0, k, T) &\equiv \epsilon(k - q_0)[\theta(q_0) + n_B(|q_0|)] \\ &\times \int_{\mathcal{R}} dq q G^{(i)}(Q) \quad (i = 1, 2) \end{aligned}$$

with $G^{(1)}(Q)$ and $G^{(2)}(Q)$ as in Eqs. (21) and (31), respectively. We compute $\mathcal{G}^{(i)}(q_0, k, T)$ ($i = 1, 2$) for various values for the parameters T and k . For the chemical potential, unless otherwise stated, we take $\mu = 350$ MeV [4].

In Figs. 4 - 8, we display the results of numerical computation for different values for k and T . The solid lines represent the total contributions $\mathcal{G} \equiv \mathcal{G}^{(1)} + \mathcal{G}^{(2)}$, while the dot-dashed lines represent $\mathcal{G}^{(1)}$. The figures “(a)” display \mathcal{G} and $\mathcal{G}^{(1)}$ in the region $q_0 \leq k$ [the region of the processes (1) and (22)] and the figures “(b)” display \mathcal{G} and $\mathcal{G}^{(1)}$ in the region $q_0 > k$ [the region of the processes (2) and (23)]. Some observations are in order.

- Figures 4 - 7 show the results for different values of k with $T = 50$ MeV. We see, as is expected, that for smaller incident-neutrino energy k , $\mathcal{G}^{(2)}/\mathcal{G}$ is larger. In the region of figures (b) [the region of the processes (2) and (23)], both $\mathcal{G}^{(1)}$ and $\mathcal{G}^{(2)}$ ($= \mathcal{G} - \mathcal{G}^{(1)}$) are positive. In the region of figures (a) [the region of the processes (1) and (22)], except for the small region $q_0 \sim 0$ (or $k' \sim k$) in the case of relatively small k/T , $\mathcal{G}^{(2)}$ is negative. Referring to the reaction-rate formula [11], one can see what kind of physical processes are involved in $d\tilde{\Gamma}_d^{(2)}/dq_0$ (Eq. (30)) and $d\tilde{\Gamma}_p^{(2)}/dq_0$ (Eq. (32)). As a matter of fact, each of them involves a set of infinite number of coherent processes. A few examples of them that are involved in $d\tilde{\Gamma}_d^{(2)}/dq_0$ are

$$\nu + e \rightarrow e + \gamma + \nu', \quad \nu + e \rightarrow e + e + e^+ + \nu'.$$

Figures 4 - 8 tell us that, for most regions displayed in figures (a), an infinite number of “interference contributions” is summed up to be negative, so that $d\tilde{\Gamma}_d^{(2)}/dq_0$ and $d\tilde{\Gamma}_p^{(2)}/dq_0$ are negative.

- Both in figures (a) and (b), $\mathcal{G}^{(2)}(q_0, k, T)$ exhibits peak structure. For figures (a) [$q_0 < k$], the peak is at $q_0 \simeq 0$ or $k' = k - q_0 \simeq k$ and is more prominent for smaller incident energy k . The structure of figures (b) [$q_0 \geq k$] may be understood as follows. In the hard-thermal-loop approximation [cf. Eq. (28)], ${}^*\Delta_F^{(T/L)}(Q) \simeq 1/[Q^2 - F_{T/L}(Q)]$ (see Eqs. (B3) and (C1)). Then, as is well known [4] or as can be shown from Eq. (B3) with Eqs. (C3) and (C4), ${}^*\Delta_{T/L}^{(12)/(21)}(Q)$ in Eq. (B2) turns out to be of the form

$$\begin{aligned}
{}^*\Delta_{T/L}^{(12)/(21)}(Q) &= 2i[\theta(\mp q_0) + n_B(|q_0|)]Z_{T/L}(q) \\
&\quad \times \delta(q_0 - \omega_{T/L}(q)) \quad (q_0 > q).
\end{aligned}
\tag{36}$$

The dispersion curves, $q_0 = \omega_T(q)$ and $q_0 = \omega_L(q)$, are schematically shown in Fig. 2. Use of the actual ${}^*\Delta_F^{T/L}(Q) = 1/[Q^2 - \Pi_F^{T/L}(Q)]$ results in the change of $\delta(q_0 - \omega_{T/L}(q))$ in Eq. (36) to the functions with finite width that are (sharply) peaked at $q_0 \simeq \omega_{T/L}(q)$. Inspection of Fig. 2 with these observation in mind allows us to understand the structure of figures (b).

For the purpose of seeing the effect of the chemical potential μ , we display in Fig. 9 the result for $(k, T, \mu) = (10, 50, 0)$ MeV. [For the QED plasma in the early universe, $\mu \simeq 0$.] We see that $\mathcal{G}^{(2)} \ll \mathcal{G}^{(1)}$, so that the peak structure is less prominent when compared to the case of $\mu = 350$ MeV, Fig. 5. \mathcal{G} in the region $q_0 > k$ is much larger than \mathcal{G} in the region $q_0 < k$.

Above computation is carried out neglecting the electron mass m_e . Inclusion of the electron mass m_e causes a change in $\Pi_F^{(S)}(Q)$ ($S = T, L, VA$) in the region $|Q^2| \leq O(m_e^2)$. For the purpose of getting a measure to what extent the approximation $m_e = 0$ is good one, we perform all numerical computations by simply cutting off the region $|Q^2| < m_e^2$. This cutoff turns out to reduce $\mathcal{G}^{(i)}$ ($i = 1, 2$). Dashed lines in Figs. 4 - 9 show the result of computation. In most regions of Figs. 4 - 9, no substantial reduction arises. Especially, for the region $q_0 \geq k$, no sizable reduction arises and we do not display the results in figures

(b). For the region $q_0 < k$, prominent reduction occurs only at $q_0 \simeq 0$, at which $\mathcal{G}^{(2)}$ peaks. Larger reduction occurs for smaller k .

B. Decay rate

For computing the contributions to the decay or damping rate $\tilde{\Gamma}_d (= \tilde{\Gamma}_d^{(1)} + \tilde{\Gamma}_d^{(2)})$ (cf. Eq. (6)) and to the production rate $\tilde{\Gamma}_p (= \tilde{\Gamma}_p^{(1)} + \tilde{\Gamma}_p^{(2)})$ (see Eq. (26)), knowledge for the distribution functions, N_ν and $N_{\bar{\nu}}$, is necessary. Furthermore, for computing the net decay rate $\Gamma_d^{\text{net}}(X; \mathbf{k})$, Eq. (33), knowledge for the distribution function $N_\nu(X; \mathbf{k})$ is necessary.

Here we compute the damping rate $\tilde{\Gamma}_d$ of an incident ν on a hot and dense QED plasma with no background neutrinos, $N_\nu = N_{\nu'} = N_{\bar{\nu}} = N_{\bar{\nu}'} = 0$. Then, the process (2) is absent. Displayed in Figs. 10 and 11 are the total contribution $\tilde{\Gamma}_d (= \tilde{\Gamma}_d^{(1)} + \tilde{\Gamma}_d^{(2)})$ and the partial contribution $\tilde{\Gamma}_d^{(1)}$ for $\mu = 350$ MeV and, in respective order, $T = 50$ MeV and 20 MeV. Figures 12 and 13 show the result for $\mu = 0$ and, in respective order, $T = 50$ MeV and 20 MeV.

Cutting off the contribution from the region $|Q^2| < m_e^2$ does not result in sizable reduction.

Characteristic features:

- For the range of k , T , and μ displayed in Figs. 10 - 13, the contribution from the soft- Q region, $\tilde{\Gamma}_d^{(2)}$, is not very large.
- Figures 12 and 13 tell us that, for $\mu = 0$, $\tilde{\Gamma}_d$ is almost linear in k . As a matter of fact, $\tilde{\Gamma}_d$'s in Figs. 12 and 13 are well parametrized as

$$\tilde{\Gamma}_d(k, T) = cG^2 k^{1+\alpha} T^{4-\alpha}$$

with $(c, \alpha) = (0.60, 0.04)$.

IV. DISCUSSIONS

On the basis of the formalism, outlined in Appendix A, for dealing with nonequilibrium quantum-field systems, we have derived the reaction-rate formulae for neutrino-conversion process and its relatives, the processes which occur in the medium that consists of a hot and dense QED plasma and background neutrinos. The formalism involves the Boltzmann equation and two related ones, which describe spacetime evolution of (anti)neutrino distribution function. Illustrative computations of the differential reaction rate $d\Gamma_{d(p)}/dq_0$ is made in Sec. IIIA and of the total decay rate Γ_d in Sec. IIIB.

For relativistic particles dealt with here, the mean-free path l is related to the decay rate Γ through $l = 1/\Gamma$ [2], which, in turn, is related to the imaginary part of the refractive index $\text{Im}[n] = (2lk)^{-1} = \Gamma/2k$. Computation in Sec.IIIB shows that, in the range of Figs. 10 and 11, order of magnitude of $\tilde{\Gamma}_d$ is $10^{-15} \sim 10^{-12}$ MeV. Then, we see from Eq. (4) that $l \simeq [0.2 \sim 200]/|U_{e\nu}^* U_{e\nu'}|^2$ m, which is much less than the core size of the type-II supernova. This means that, when applying to the actual supernova, $\bar{\nu}\nu'$ as well as $\nu\bar{\nu}'$ production processes are also important and, through these processes, (anti)neutrinos are produced. Thus, one has to perform an analysis by the full use of the formalism in Appendix A. The evolution of the neutrino- and antineutrino-distribution functions should be dealt with through the Boltzmann equation and its relatives. Once the initial distribution function of (anti)neutrinos are given, the framework presented here allows one to determine hereafter of the system. Concrete numerical analysis along this line is outside of the scope of the present paper.

ACKNOWLEDGMENTS

The authors thank T. Hatsuda for useful comments. M. K. contributed to this work at the early stage. A. Niégawa was supported in part by a Grant-in-Aide for Scientific Research ((C)(2) (No. 12640287)) of the Ministry of Education, Science, Sports and Culture of Japan.

**APPENDIX A: NONEQUILIBRIUM NEUTRINO PROPAGATOR AND
“HEALTHY” PERTURBATION THEORY**

A perturbative framework for dealing with massless Dirac fermions in a nonequilibrium quantum-field system is presented in [12]. Extension of the framework to the case of massless left-handed neutrino ν_L is straightforward. Here we briefly describe somewhat simpler framework for ν_L , which is sufficient for the present purpose. We employ the derivative expansion and use the gradient approximation throughout.

1. Free propagator

We start with introducing a standard form [13,12] for nonequilibrium matrix propagator of a massless left-handed neutrino ν_L :

$$\begin{aligned}\hat{S}_\nu(x, y) &= \int \frac{d^4u}{(2\pi)^4} \int \frac{d^4v}{(2\pi)^4} \hat{B}_L(x, u) \\ &\quad \times \hat{S}_{RA}(u - v) \hat{B}_R(v, y), \\ \hat{B}_L(x, y) &= \begin{pmatrix} \delta^4(x - y) & -f_\nu(x, y) \\ \delta^4(x - y) & \delta^4(x - y) - f_\nu(x, y) \end{pmatrix}, \\ \hat{B}_R(x, y) &= \begin{pmatrix} \delta^4(x - y) - f_\nu(x, y) & -f_\nu(x, y) \\ \delta^4(x - y) & \delta^4(x - y) \end{pmatrix}, \\ \hat{S}_{RA} &= \text{diag}(S_R, -S_A).\end{aligned}\tag{A1}$$

Here “ $\hat{}$ ” denotes a 2×2 matrix in a “type space.” In a 4×4 Dirac-matrix space, \hat{B}_L and \hat{B}_R are the unit matrices. The Fourier transform of $S_{R(A)}$ reads

$$S_{R(A)}(P) = L \not{P} \Delta_{R(A)}(P) \quad (L = (1 - \gamma_5)/2),$$

where $\Delta_{R(A)}(P)$ is as in Eq. (10) and $f_\nu(x, y)$ is the inverse Wigner transform of

$$\begin{aligned}f_\nu(X; P) &= \theta(p_0) N_\nu(X; p_0, \mathbf{p}) \\ &\quad + \theta(-p_0) [1 - N_{\bar{\nu}}(X; |p_0|, -\mathbf{p})]\end{aligned}$$

with $X = (x + y)/2$. Here N_ν ($N_{\bar{\nu}}$) is the number-density function of ν ($\bar{\nu}$). Computation of Eq. (A1) to the gradient approximation yields

$$\begin{aligned}\hat{S}_\nu(x, y) &= \int \frac{d^4 P}{(2\pi)^4} e^{-iP \cdot (x-y)} \hat{S}_\nu\left(\frac{x+y}{2}; P\right), \\ \hat{S}_\nu(X; P) &= \hat{S}_\nu^{(0)}(X; P) + \hat{S}_\nu^{(1)}(X; P).\end{aligned}$$

The leading term $\hat{S}_\nu^{(0)}$ is given by Eq. (9) with ν for ν' and the nonleading term $\hat{S}_\nu^{(1)}$ reads

$$\hat{S}_\nu^{(1)} = -iL\hat{A}_+ \left[(\not{\partial}_X f_\nu) \frac{\mathbf{P}}{P^2} + 2(P \cdot \partial_X f_\nu) \not{P} \frac{\partial}{\partial P^2} \frac{\mathbf{P}}{P^2} \right], \quad (\text{A2})$$

where \hat{A}_+ is as in Eq. (12) and \mathbf{P} denotes principal part.

2. Free and counter actions

The propagator introduced above is an inverse of the kernel of a free action A_0 , which we now find. Applying $\not{\partial}_x$ to $\hat{S}_\nu(x, y)$ in Eq. (A1), we find the form of A_0 , to the gradient approximation:

$$A_0 = \int d^4 x \bar{\Psi}(x) i\not{\partial} L \Psi(y) - A_C, \quad (\text{A3})$$

$$\bar{\Psi} = (\bar{\psi}_1, \bar{\psi}_2), \quad \Psi(x) = \begin{pmatrix} \psi_1 \\ \psi_2 \end{pmatrix}, \quad (\text{A4})$$

$$\begin{aligned}A_C &= \int \frac{d^4 x}{(2\pi)^4} \int \frac{d^4 y}{(2\pi)^4} \bar{\Psi}(x) \\ &\quad \times (i\not{\partial}_x + i\not{\partial}_y) L f_\nu(x, y) \hat{A}_- \Psi(y),\end{aligned} \quad (\text{A5})$$

where \hat{A}_- is as in Eq. (12). In Eq. (A4), the subscripts of the field denote the type of field in real-time formalism [10]. From Eq. (A3), we see that the action of the theory turns out to be

$$A = A_0 + A' + A_c,$$

where A' includes other fields than ν_L and $\bar{\nu}_L$ and the interactions between fields. It is to be noted that the counter action A_c appears.

3. Self-energy part and “healthy” perturbation theory

The self-energy-part matrix of ν reads

$$\hat{\Sigma}_\nu(X; P) = \hat{\Sigma}_\nu^{(\text{loop})}(X; P) - i\hat{\not{\partial}}_X f(X; P)L\hat{A}_-,$$

where $\hat{\Sigma}_\nu^{(\text{loop})}$ comes from loop diagrams and the second term on the RHS comes from the counter action A_c . Computation of a $\hat{\Sigma}$ -inserted propagator to the leading order of derivative expansion yields

$$\begin{aligned} & \hat{S}_\nu(X; P)\hat{\Sigma}_\nu(X; P)\hat{S}_\nu(X; P) \\ &= -iS_R \left[\left(\hat{\not{\partial}}_X f_\nu \right) L \right. \\ & \quad \left. -i \left\{ (1 - f_\nu)\Sigma_{12}^{(\nu)} + f_\nu\Sigma_{21}^{(\nu)} \right\} S_A \hat{A}_+ \right. \\ & \quad \left. + \dots \right] \end{aligned}$$

Here $f_\nu = f_\nu(X; P)$ and “...” contains the terms with $S_R\Sigma_R^{(\nu)}S_R$ and with $S_A\Sigma_A^{(\nu)}S_A$, where $\Sigma_{R(A)}^\nu = \Sigma_{11}^\nu + \Sigma_{12(21)}^\nu$ is the retarded (advanced) self-energy part [10]. Observing $S_RS_A \propto 1/[(P^2 + i0^+)(P^2 - i0^+)]$, we see that S_RS_A possesses pinch singularities at $p_0 = \pm p$ in a complex p_0 -plane. Then, by demanding**

$$\begin{aligned} & \hat{\not{\partial}}_X f_\nu(X; P)L = F_\nu(X; P), \\ & F_\nu(X; P) = i \left[(1 - f_\nu)\Sigma_{12}^{(\nu)} + f_\nu\Sigma_{21}^{(\nu)} \right], \end{aligned} \tag{A6}$$

we attain a pinch-singularity free perturbation theory.

4. Boltzmann equation and its relative equations

After multiplying $L\not{P}$ from the left of Eq. (A6), we take a trace and go on the mass-shell $p_0 = \pm p$. Referring to Eqs. (5) and (25) together with their antiparticle counterparts, we obtain, with obvious notation,

**As a matter of fact, demanding Eq. (A6) to hold in any region(s) of P will do, as far as $p_0 = +p$ and $p_0 = -p$ are within that region(s).

$$\begin{aligned}
& (\partial_{X_0} + \mathbf{v} \cdot \nabla_X) N_{\pm}(X; p, \mathbf{p}) \\
&= (1 - N_{\pm}(X; p, \mathbf{p})) \Gamma_p^{(\pm)}(X; \mathbf{p}) \\
&\quad - N_{\pm}(X; p, \mathbf{p}) \Gamma_d^{(\pm)}(X; \mathbf{p}).
\end{aligned} \tag{A7}$$

Here $\mathbf{v} \equiv \mathbf{p}/p$ and “+” [“−”] stands for ν [$\bar{\nu}$]. As can be seen from Eq. (33), the RHS is the net production rate of $\nu/\bar{\nu}$ and Eq. (A7) is nothing but the Boltzmann equation.

Similarly, multiplications of $L\gamma^0$ and of $L\vec{\gamma}_{\perp}$ ($= L\vec{\gamma} - L(\vec{\gamma} \cdot \hat{\mathbf{p}})\hat{\mathbf{p}}$) to Eq. (A6) yields, in respective order,

$$\partial_{X_0} N_{\pm}(X; p, \mathbf{p}) = \pm \frac{1}{2} \text{Tr} [L\gamma^0 F_{\nu}]_{p_0=\pm p, \mathbf{p} \rightarrow \pm \mathbf{p}}, \tag{A8}$$

$$\vec{\gamma}_{\perp} \cdot \nabla_X N_{\pm}(X; p, \mathbf{p}) = \pm \frac{1}{2} \text{Tr} [L\vec{\gamma}_{\perp} F_{\nu}]_{p_0=\pm p, \mathbf{p} \rightarrow \pm \mathbf{p}}. \tag{A9}$$

If (initial) distributions are spatially isotropic, the RHS of Eq. (A9) vanishes.

APPENDIX B: SELF-ENERGY-PART RESUMMED PROPAGATOR OF A PHOTON

Elements of the self-energy-part-resummed photon propagator matrix (in Landau gauge) reads [4,5,9]

$$\begin{aligned}
{}^* \Delta_{ij}^{\alpha\beta}(Q) &= -\mathcal{P}_T^{\alpha\beta}(\hat{\mathbf{q}}) {}^* \Delta_T^{(ij)}(Q) - \mathcal{P}_L^{\alpha\beta}(Q) {}^* \Delta_L^{(ij)}(Q) \\
&\quad (i, j = 1, 2),
\end{aligned} \tag{B1}$$

where $\mathcal{P}_T^{\alpha\beta}(\hat{\mathbf{q}})$ and $\mathcal{P}_L^{\alpha\beta}(Q)$ are as in Eq. (16) and

$$\begin{aligned}
{}^* \Delta_{T/L}^{(11)}(Q) &= - \left({}^* \Delta_{T/L}^{(22)}(Q) \right)^* \\
&= {}^* \Delta_F^{(T/L)}(Q) + 2in_B(|q_0|) \text{Im} {}^* \Delta_F^{(T/L)}(Q), \\
{}^* \Delta_{T/L}^{(12)/(21)}(Q) &= 2i[\theta(\mp q_0) + n_B(|q_0|)] \text{Im} {}^* \Delta_F^{(T/L)}(Q),
\end{aligned} \tag{B2}$$

$${}^* \Delta_F^{(T/L)}(Q) = \frac{1}{Q^2 - \Pi_F^{(T/L)}(Q)}. \tag{B3}$$

$\Pi_F^{(T/L)}$ is computed to the one-loop order in Appendix C.

APPENDIX C: SELF-ENERGY PART $\Pi_F^{(S)}$ ($S = T, L, VA$)

Here we compute the lowest-order contribution to $\Pi_F^S(Q)$ ($S = T, L, VA$), Eq. (17). We are interested in the high- T and large- μ region $T, \mu \gg m_e$, and then we ignore m_e . The effect of m_e ($\neq 0$) is discussed in Sec. III.

Computation of $\Pi_F^{(S)}(Q)$ ($S = T, L, VA$)

We decompose $\Pi_F^{(T)}(Q)$ and $\Pi_F^{(L)}(Q)$ into three parts,

$$\Pi_F^{(T/L)}(Q) = F_{T/L}^{(0)}(Q) + F_{T/L}(Q) + G_{T/L}(Q). \quad (\text{C1})$$

$F_{T/L}^{(0)}$ stands for the vacuum contribution and $F_{T/L}$ stand for the contributions that dominate in the soft- Q region, the latter contributions which are called hard thermal loop [4,5]. Incidentally, $\Pi_F^{(VA)}(Q)$ has no hard thermal loop.

Straightforward computation of Eq. (17) (cf. Eqs. (8), (15), and (16)) using Eqs. (13) and (14) yields

$$F_T^{(0)}(Q) = F_L^{(0)}(Q) = -\frac{\alpha}{3\pi} Q^2 \left[\frac{5}{3} - \ln \left(\frac{-Q^2}{\mu_r^2} \right) \right], \quad (\text{C2})$$

$$F_T(Q) = \frac{3}{2} m_\gamma^2 \frac{q_0}{q} \left[\frac{q_0}{q} - \frac{Q^2}{2q^2} \ln \frac{q_0 + q}{q_0 - q} \right], \quad (\text{C3})$$

$$F_L(Q) = -3 m_\gamma^2 \frac{Q^2}{q^2} \left[1 - \frac{q_0}{2q} \ln \frac{q_0 + q}{q_0 - q} \right], \quad (\text{C4})$$

$$G_T(Q) = -\frac{\alpha}{\pi} Q^2 \left[\left(1 + \frac{Q^2}{2q^2} \right) I_1 + \frac{2}{q^2} (I_2 - q_0 I_3) \right], \quad (\text{C5})$$

$$G_L(Q) = \frac{\alpha}{\pi} \frac{Q^2}{q^2} \left[Q^2 I_1 + 4 (I_2 - q_0 I_3) \right], \quad (\text{C6})$$

and

$$\Pi_F^{(VA)} = -\frac{e^2}{4\pi^2} \frac{Q^2}{q^3} \left[\mu q_0 \ln \frac{q_0 + q}{q_0 - q} - q q_0 \tilde{I}_3 + 2q \tilde{I}_1 \right]. \quad (\text{C7})$$

In obtaining the vacuum contribution (C2), we have used the $\overline{\text{MS}}$ scheme^{††} and μ_r is the renormalization scale, for which we choose $\mu_r = \sqrt{T^2 + \mu^2}$. Incidentally, the vacuum part of $\Pi_F^{(VA)}$ vanishes. In the above equations, $\alpha = e^2/4\pi$, $m_\gamma^2 = e^2(T^2 + 3\mu^2/\pi^2)/9$ is the thermal mass of an electron, and

$$I_1 \equiv -\frac{1}{2q} \int_0^\infty dp [n_+(p) + n_-(p)] \ln \left(\frac{L_{++} L_{--}}{L_{+-} L_{-+}} \right), \quad (\text{C8})$$

$$I_2 \equiv \frac{\pi^2}{6} \left(T^2 + \frac{3\mu^2}{\pi^2} \right) - \frac{1}{2q} \int_0^\infty dp p^2 [n_+(p) + n_-(p)] \ln \left(\frac{L_{++} L_{--}}{L_{+-} L_{-+}} \right), \quad (\text{C9})$$

$$I_3 \equiv \frac{1}{2q} \int_0^\infty dp p [n_+(p) + n_-(p)] \ln \left(\frac{L_{++} L_{+-}}{L_{-+} L_{--}} \right), \quad (\text{C10})$$

$$\tilde{I}_1 \equiv -\frac{1}{2q} \int_0^\infty dp p [n_+(p) - n_-(p)] \ln \left(\frac{L_{++} L_{--}}{L_{+-} L_{-+}} \right), \quad (\text{C11})$$

$$\tilde{I}_3 \equiv \frac{1}{2q} \int_0^\infty dp [n_+(p) - n_-(p)] \ln \left(\frac{L_{++} L_{+-}}{L_{-+} L_{--}} \right) \quad (\text{C12})$$

with

$$n_\pm(p) = 1/(e^{(p \mp \mu)/T} + 1),$$

$$L_{\rho\sigma} \equiv q_0 + \rho q + 2\sigma p \quad (\rho, \sigma = \pm).$$

It is straightforward to obtain

$$\text{Im}\Pi_F^{(T/L)}(Q) \equiv \frac{1}{2i} \left[\Pi_F^{(T/L)}(q_0(1 + i\epsilon), q) - \text{c.c.} \right], \quad (\text{C13})$$

$$\text{Im}F_T(Q) = \theta(-Q^2) \frac{3\pi}{4} m_\gamma^2 Q^2 \frac{|q_0|}{q^3}, \quad (\text{C14})$$

^{††}We have adopted a convention that Dirac gamma matrices are 4×4 matrices in D -dimensional spacetime.

$$\text{Im} \left(\frac{F_L(Q)}{Q^2} \right) = -\theta(-Q^2) \frac{3\pi}{2} m_\gamma^2 \frac{|q_0|}{q^3}, \quad (\text{C15})$$

$$\text{Im} I_1 = -\frac{\pi T}{2q} (F_{--} + F_{+-} - F_{-+} - F_{++}), \quad (\text{C16})$$

$$\text{Im} I_2 = -\frac{\pi}{2q} \int_{q_l}^{q_u} dp p^2 [n_+(p) + n_-(p)], \quad (\text{C17})$$

$$\begin{aligned} \text{Im} I_3 = & -\frac{\pi}{2q} \epsilon(q_0) \int_{q_l}^{q_u} dp p [n_+(p) + n_-(p)] \\ & -\frac{\pi}{q} \epsilon(q_0) \theta(-Q^2) \\ & \times \int_0^{q_l} dp p [n_+(p) + n_-(p)], \end{aligned} \quad (\text{C18})$$

$$\text{Im} \tilde{I}_1 = -\frac{\pi}{2q} \int_{q_l}^{q_u} dp p [n_+(p) - n_-(p)], \quad (\text{C19})$$

$$\begin{aligned} \text{Im} \tilde{I}_3 = & \frac{\pi}{q} \epsilon(q_0) \theta(-Q^2) \mu \\ & -\frac{\pi}{2q} \epsilon(q_0) T [F_{++} - F_{-+} \\ & -\epsilon(Q^2) (F_{+-} - F_{--})], \end{aligned} \quad (\text{C20})$$

where

$$\begin{aligned} q_u &\equiv \frac{|q_0| + q}{2}, & q_l &\equiv \frac{||q_0| - q|}{2}, \\ F_{\rho\sigma} &= \ln \left(e^{\rho\mu/T} + e^{-||q_0| + \sigma q|/(2T)} \right) \quad (\rho, \sigma = +, -). \end{aligned} \quad (\text{C21})$$

Note that $\Pi_F^{(VA)}(Q)$ vanishes for $\mu = 0$.

REFERENCES

- [1] Proc. 16th Workshop on Weak Interactions and Neutrinos (WIN 97), Capri, Italy, 22-28 June 1997, eds., G. Fiorillo, V. Palladino, and P. Strolin, Nucl. Phys. B (Proc. Suppl.) **66** (1998) July 1998; R. D. Peccei, *Neutrino Physics*, hep-ph/9906509; M. Prakash, J. M. Lattimer, R. F. Sawyer, and R. R. Volkas, Ann. Rev. Nucl. Part. Sci. 51 (2001).
- [2] D. Nötzold and G. Raffelt, Nucl. Phys. **B307**, 924 (1988).
- [3] J. C. D’Olivo, J. F. Nieves, and P. B. Pal, Phys. Rev. D **40**, 3679 (1989); J. C. D’Olivo, J. F. Nieves, and P. B. Pal, Phys. Rev. Lett. **64**, 1088 (1990); J. F. Nieves and P. B. Pal, Phys. Rev. D **56**, 365 (1997); D. Grasso and V. Semikoz, *ibid.* D **60**, 053010 (1999). See also, C. Giunti, C. W. Kim, and W. P. Lam, Phys. Rev. D **43**, 164 (1991).
- [4] M. Le Bellac, *Thermal Field Theory* (Cambridge Univ. Press, Cambridge, 1996).
- [5] R. D. Pisarski, Phys. Rev. Lett. **63**, 1129 (1989); E. Braaten and R. D. Pisarski, Nucl. Phys. **B337**, 569 (1990); **339**, 310 (1990); J. Frenkel and J. C. Taylor, *ibid.* **334**, 199 (1990).
- [6] A. Ayala, J. C. D’Olivo, and M. Torres, Phys. Rev. D **59**, 111901 (1999); Nucl. Phys. **B564**, 204 (2000).
- [7] E. Roulet, Lectures given at the: Summer School on Astroparticle Physics and Cosmology, Trieste, June 2000, hep-ph/0011570.
- [8] A. de Gouvêa and J. W. F. Valle, Phys. Lett. **B501**, 115 (2001).
- [9] N. P. Landsman and Ch. G. van Weert, Phys. Rep. **145**, 141 (1987).
- [10] K.-C. Chou, Z.-B. Su, B.-L. Hao, and L. Yu, Phys. Rep. **118**, 1 (1985). See also, P. A. Henning, Phys. Rep. **253**, 235 (1995).
- [11] A. Niégawa, Phys. Rev. D **57**, 1379 (1998); A. Niégawa, K. Okano, and H. Ozaki, *ibid.* **61**, 056004 (2000).

- [12] A. Niégawa, hep-ph/0101216; J.-P. Blaizot and E. Iancu, hep-ph/0101103; P. A. Henning in [10]. For other fields than the fermion, see, A. Niégawa, Prog. Theor. Phys. **102**, 1 (1999); Phys. Rev. D **62**; 125004 (2000); *ibid.* **64**, 036004 (2001); J.-P. Blaizot and E. Iancu, Nucl. Phys. **B557**, 183 (1999).
- [13] H. Umezawa, “Advanced Field Theory — Micro, Macro, and Thermal Physics.” AIP, New York, 1993; H. Chu and H. Umezawa, Int. J. Mod. Phys. **A9**, 1703 and 2363 (1994) and earlier papers quoted therein.

FIGURES

FIG. 1. Diagram for $\tilde{\Gamma}_d^{(1)}$. “1” (“2”) at the vertex on the left-side (right-side) denotes the type of vertex in real-time equilibrium/nonequilibrium quantum field theory. The oval loop is an electron loop.

FIG. 2. Integration region $\mathcal{R} = \mathcal{R}_1 \cup \mathcal{R}_2$. The dashed line with T (L) shows the dispersion relation for the transverse (longitudinal) mode in the hard-thermal-loop resummed photon propagator.

FIG. 3. Diagram for $\tilde{\Gamma}_d^{(2)}$. The hard-thermal-loop resummed effective photon propagator is indicated by a blob. “1”, “2”, “ i ”, and “ j ” on the vertexes denote the type of vertex. The oval loops are electron loops.

FIG. 4. Plots of \mathcal{G} and $\mathcal{G}^{(1)}$ vs q_0 at $T = 50$ MeV, $\mu = 350$ MeV, and $E = 2$ MeV. Figure (a) corresponds to the processes (1) and (22), and Fig. (b) corresponds to the processes (2) and (23).

FIG. 5. Same as in Fig. 4 but for $E = 10$ MeV.

FIG. 6. Same as in Fig. 4 but for $E = 20$ MeV.

FIG. 7. Same as in Fig. 4 but for $E = 50$ MeV.

FIG. 8. Same as in Fig. 4 but for $T = 20$ MeV and $E = 10$ MeV.

FIG. 9. Same as in Fig. 4 but for $\mu = 0$ and $E = 10$ MeV.

FIG. 10. Plots of $\tilde{\Gamma}_d$ and $\tilde{\Gamma}_d^{(1)}$ vs E at $T = 50$ MeV and $\mu = 350$ MeV.

FIG. 11. Same as in Fig. 10 but for $T = 20$ MeV.

FIG. 12. Plots of $\tilde{\Gamma}_d$ and $\tilde{\Gamma}_d^{(1)}$ vs E at $T = 50$ MeV and $\mu = 0$.

FIG. 13. Same as in Fig. 12 but for $T = 20$.

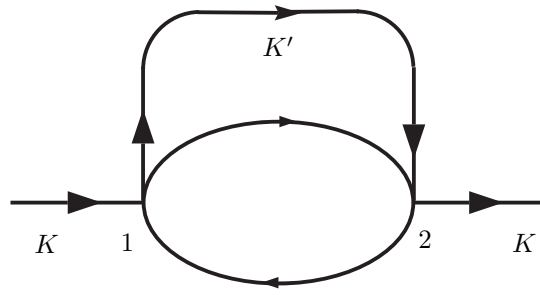


FIG. 1

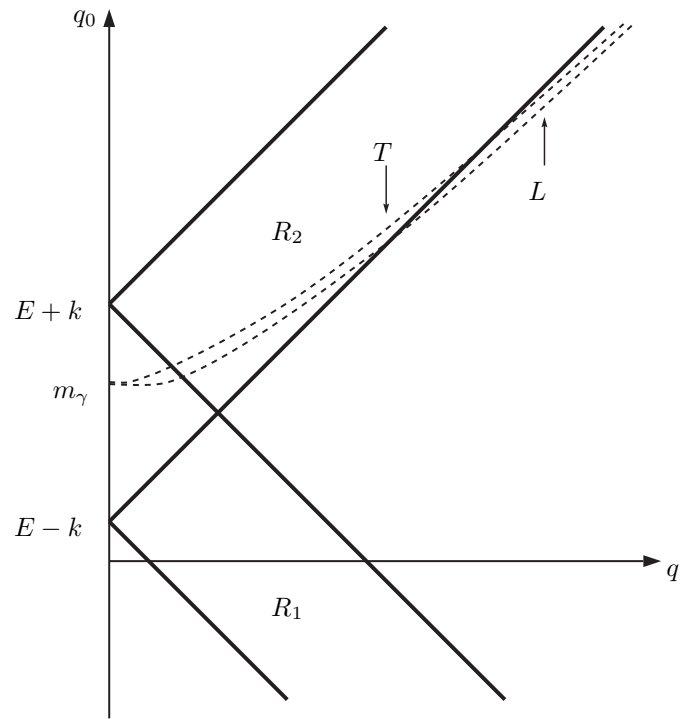


Fig. 2

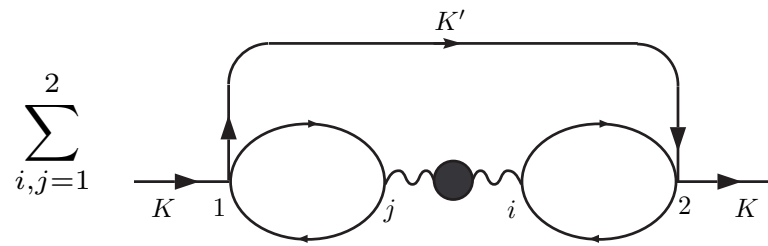
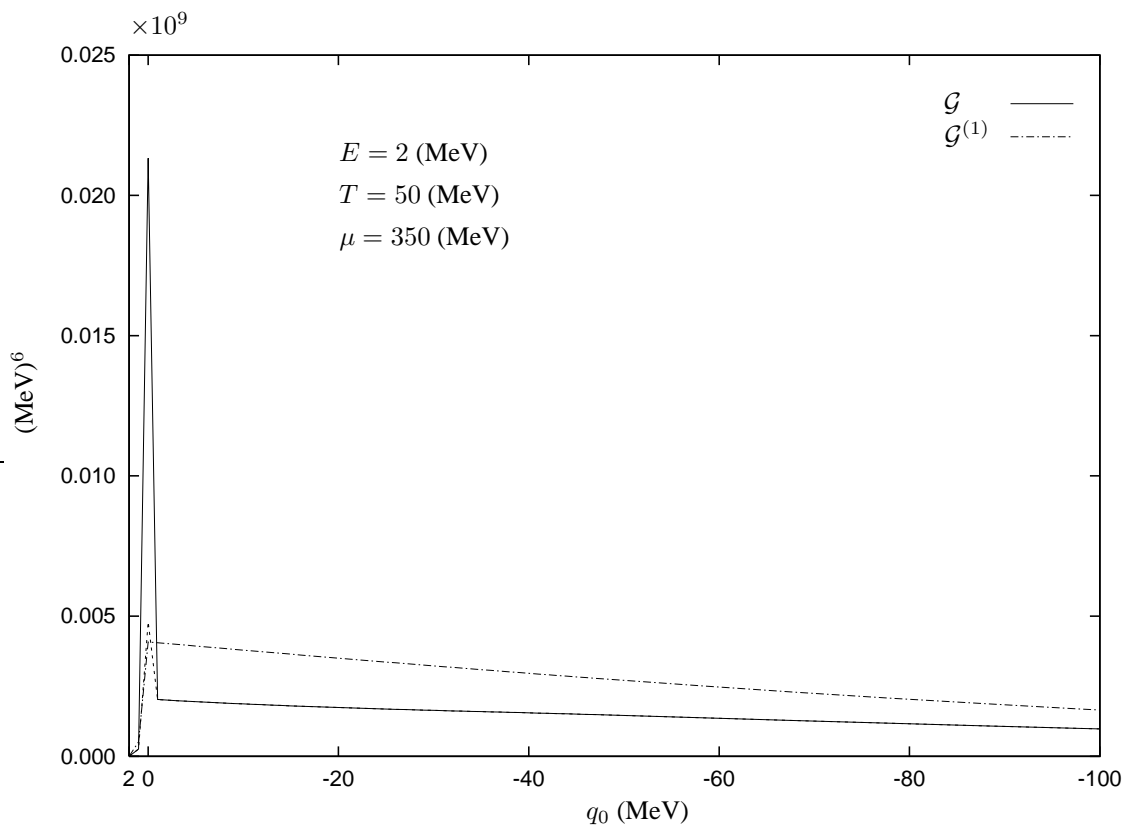
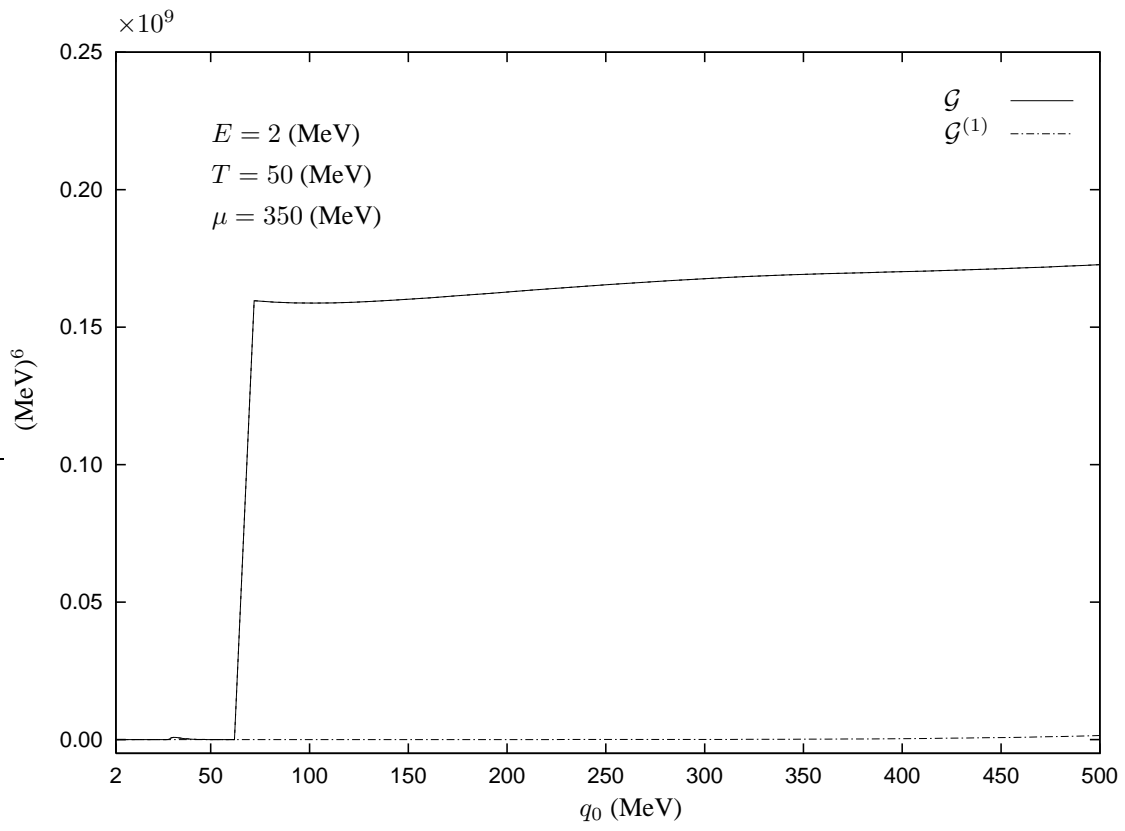


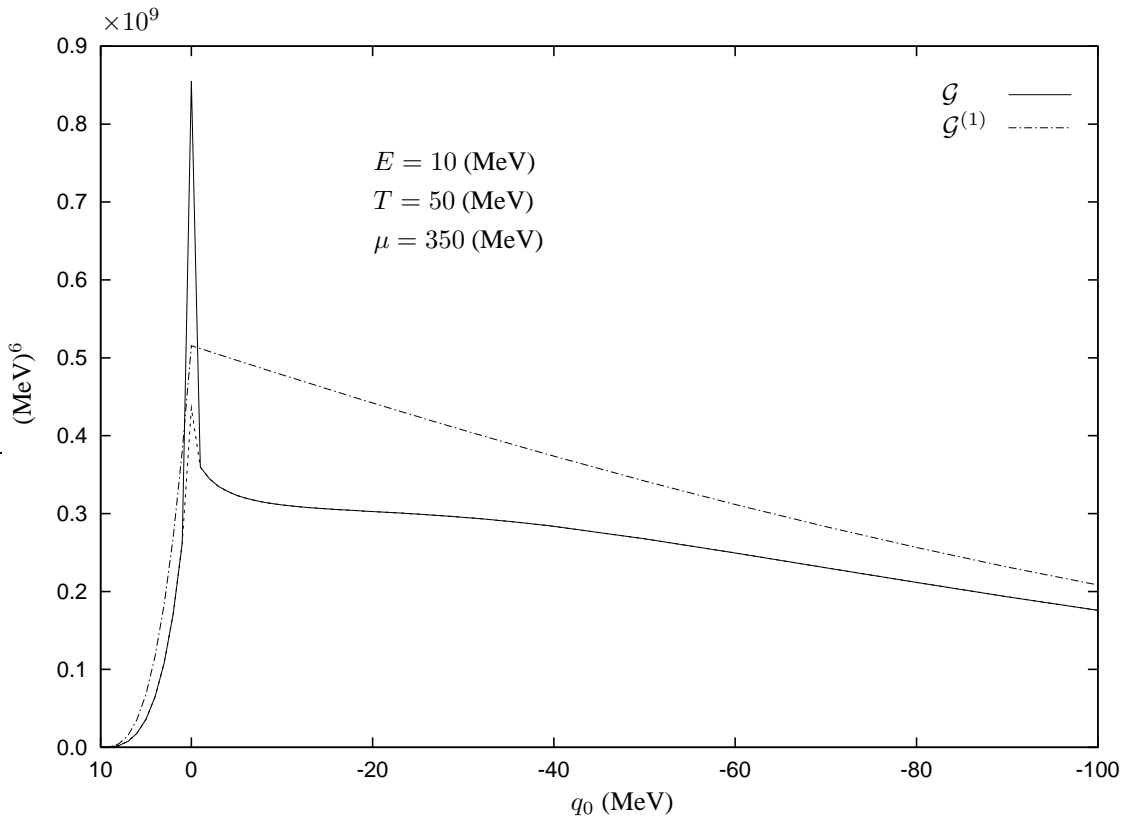
FIG. 3



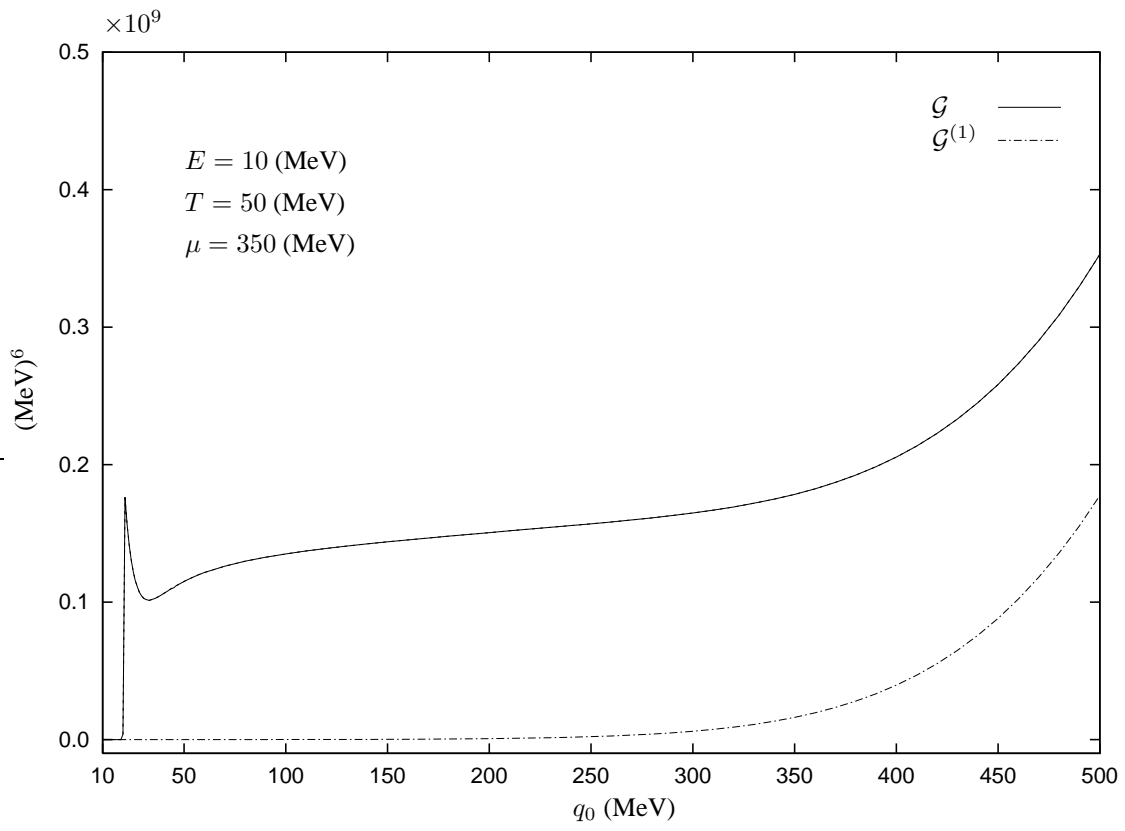
4(a)



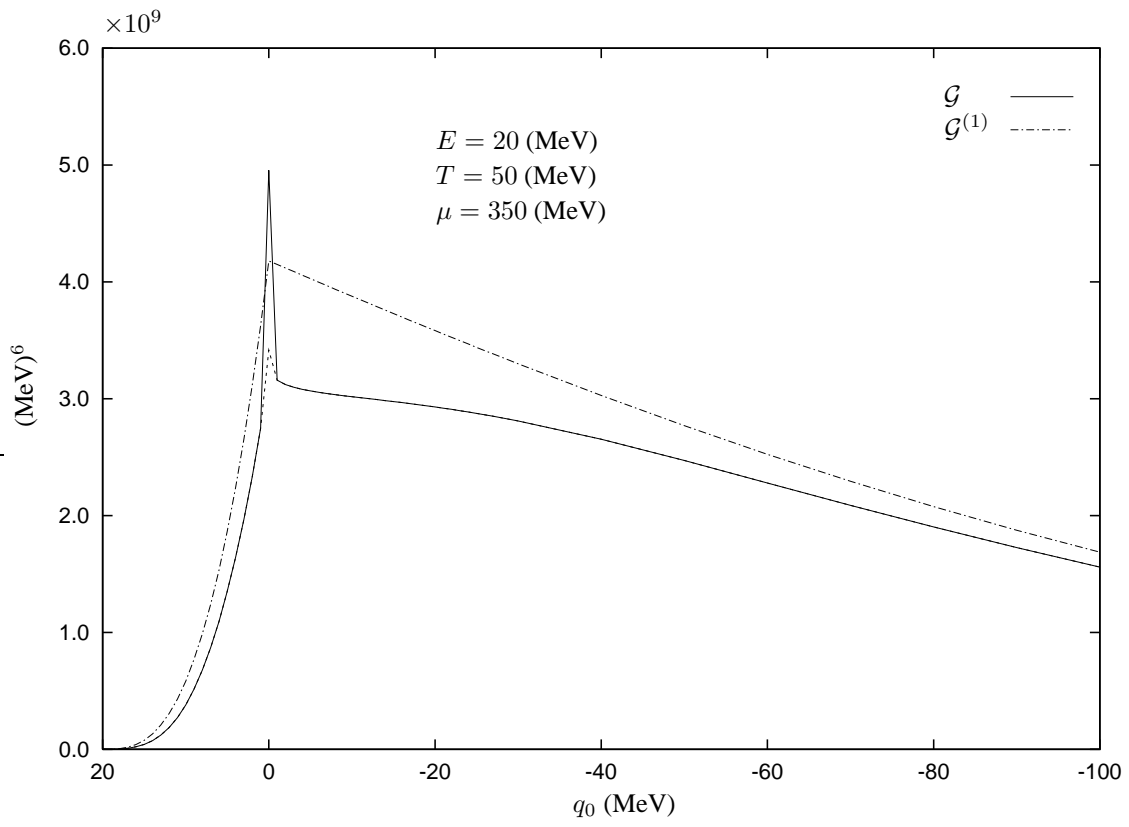
4(b)



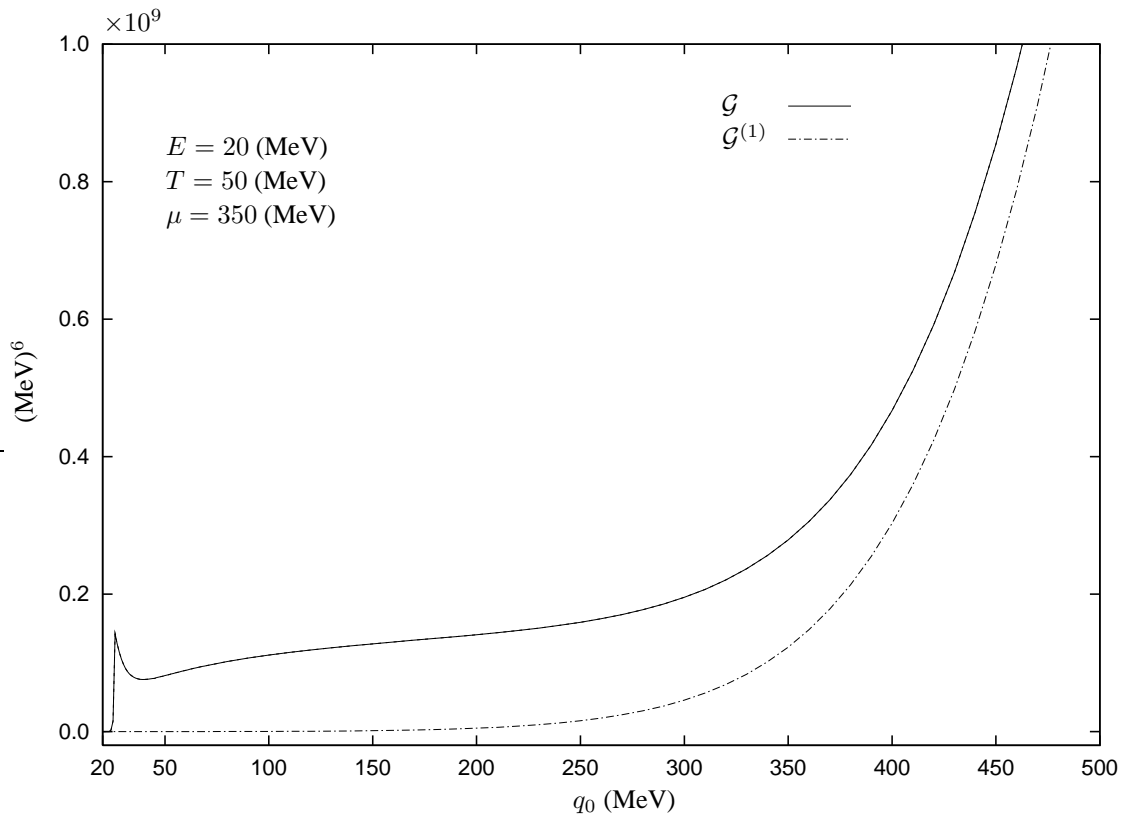
5(a)



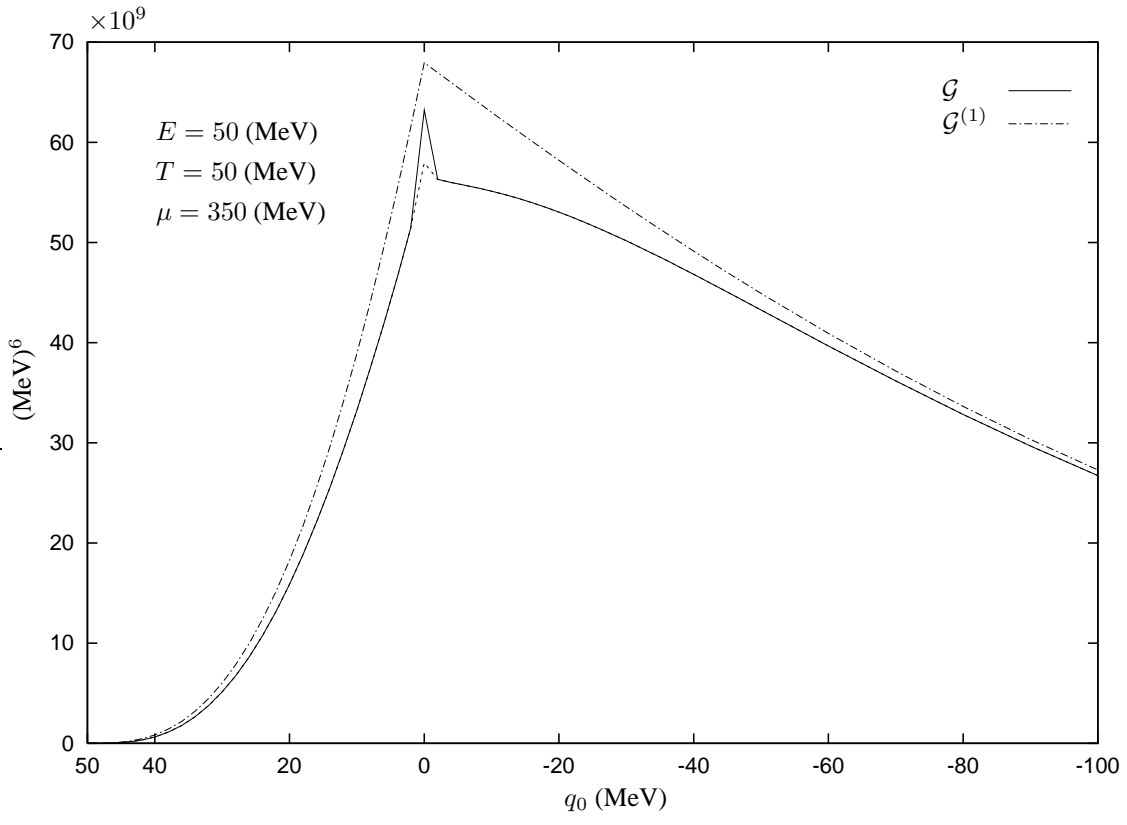
5(b)



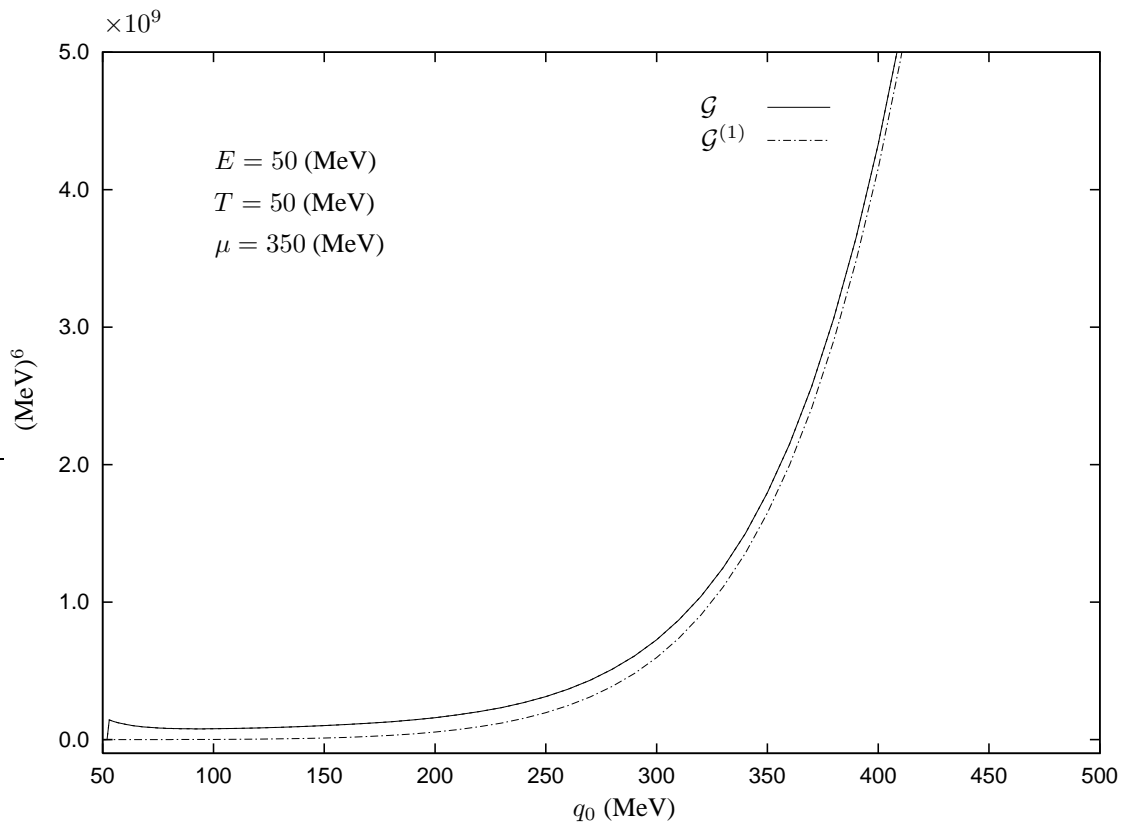
6(a)



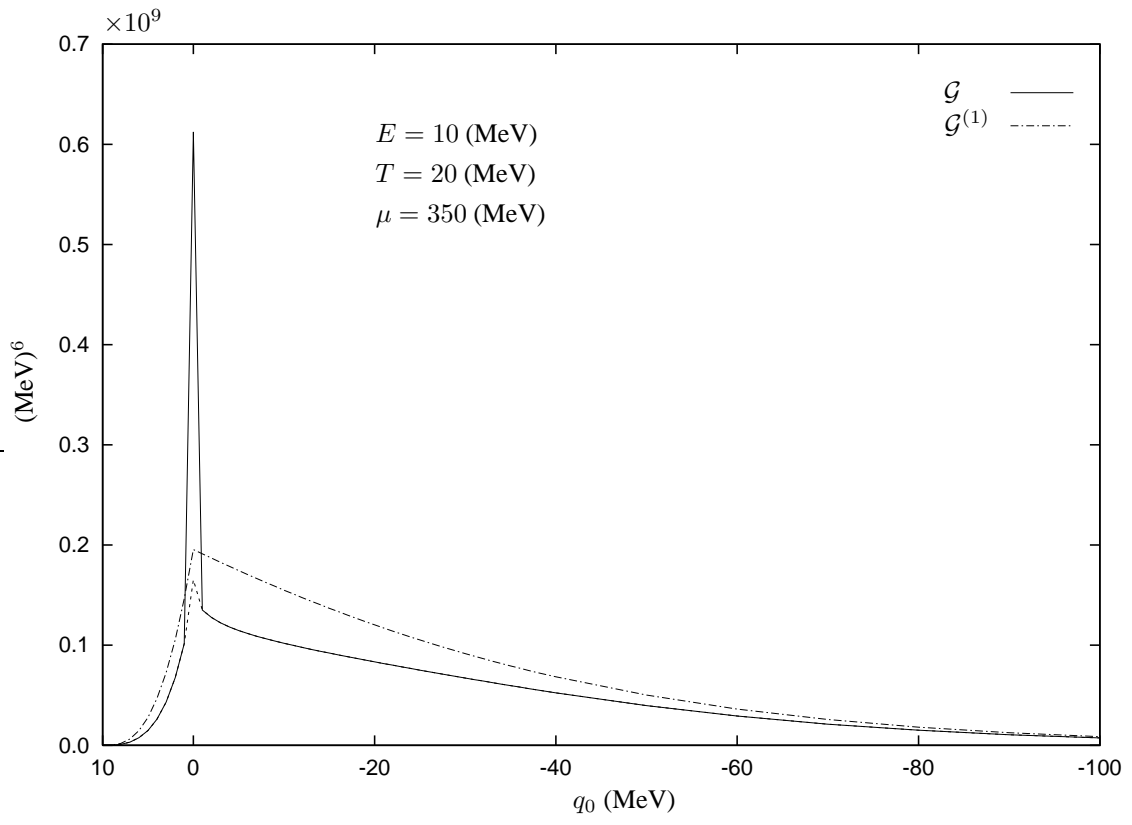
6(b)



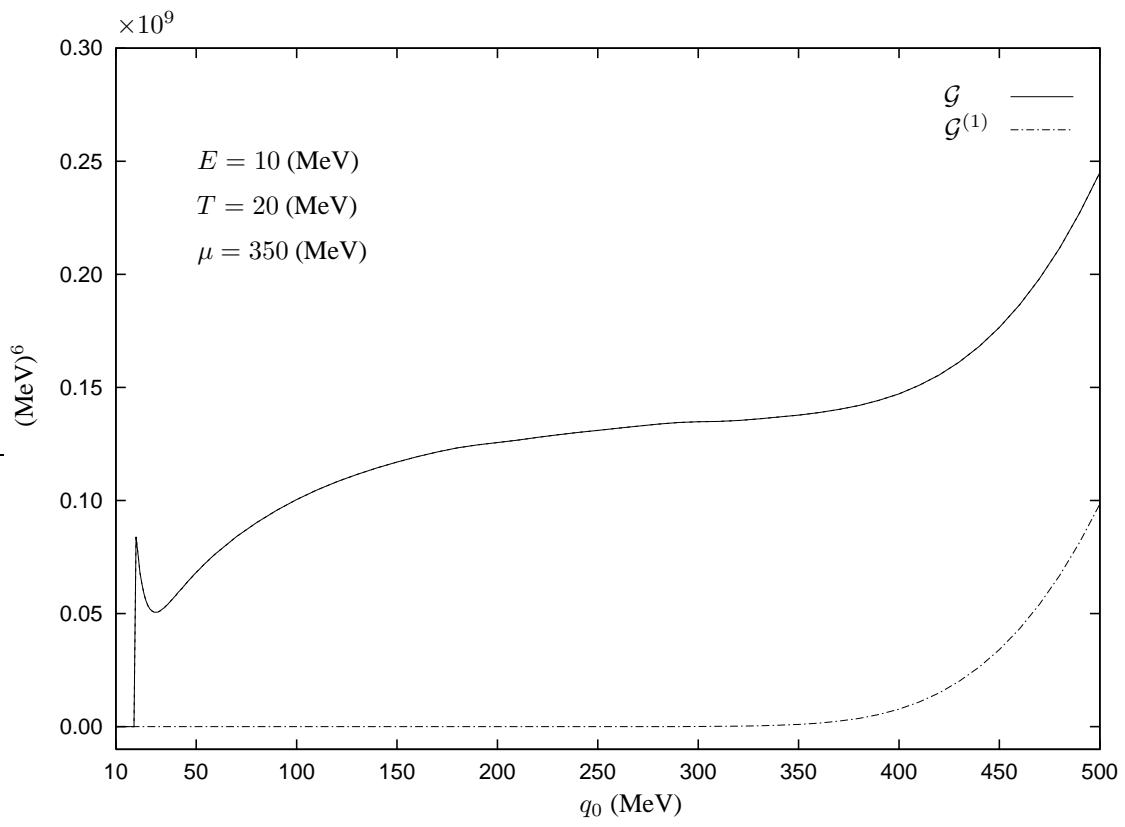
7(a)



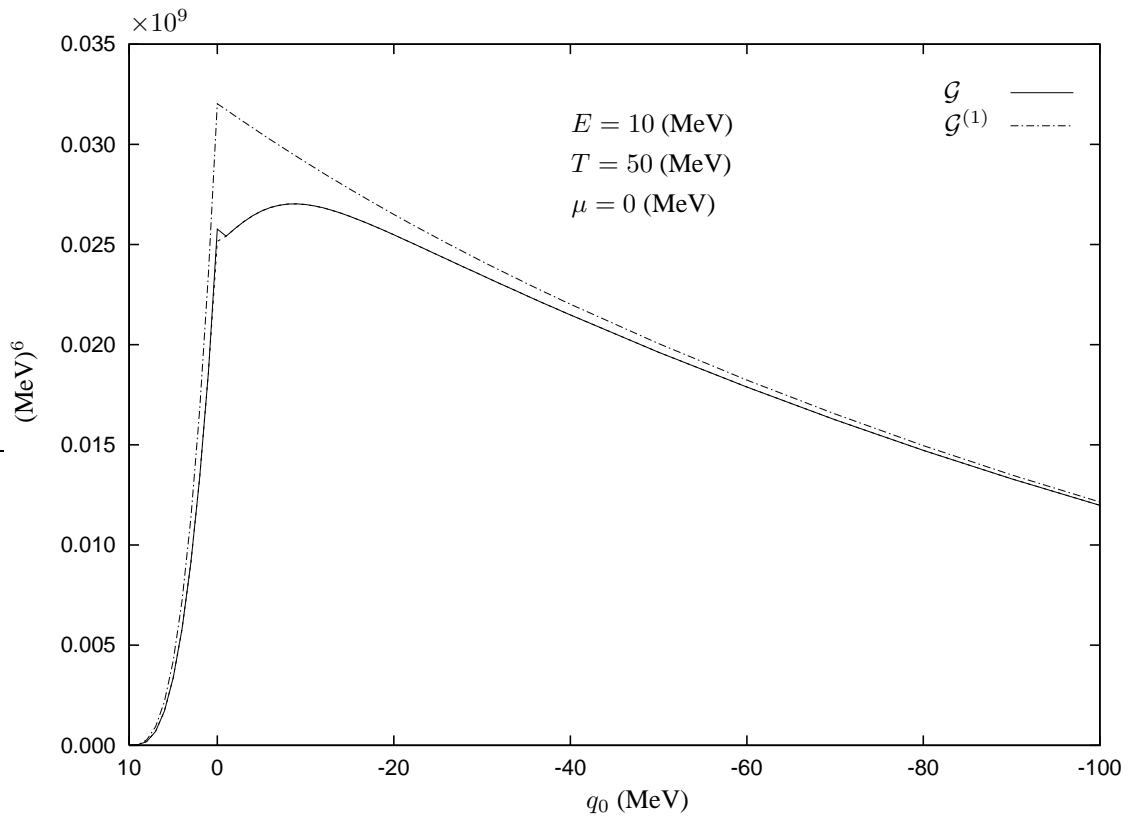
7(b)



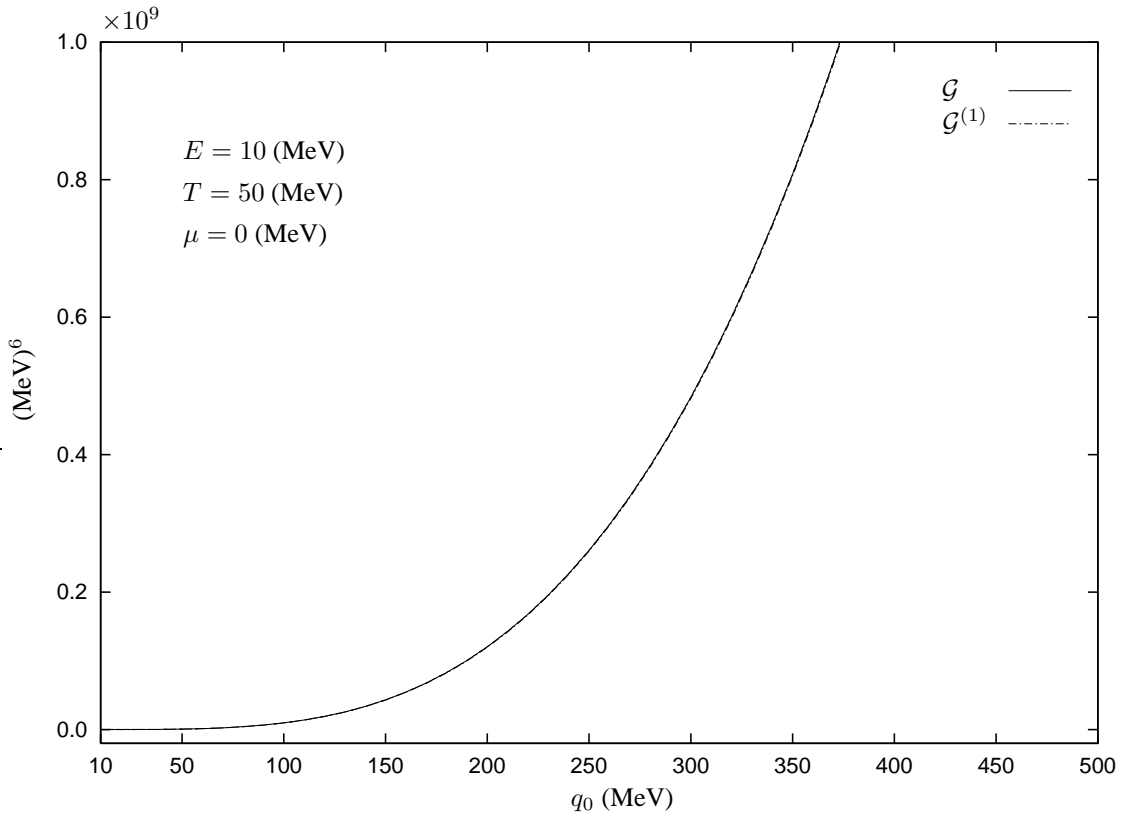
8(a)



8(b)



9(a)



9(b)

